Physics Letters B 663 (2008) 228–233

Contents lists available at ScienceDirect

Physics Letters B

www.elsevier.com/locate/physletb

Bound diquarks and their Bose–Einstein condensation in strongly coupled quark matter

Masakiyo Kitazawa [a,*], Dirk H. Rischke [b], Igor A. Shovkovy [c]

[a] Department of Physics, Osaka University, Toyonaka, Osaka 560-0043, Japan
[b] Institut für Theoretische Physik and Frankfurt Institute for Advanced Studies, J.W. Goethe-Universität, D-60438 Frankfurt am Main, Germany
[c] Western Illinois University, Macomb, IL 61455, USA

ARTICLE INFO

Article history:
Received 18 September 2007
Received in revised form 30 January 2008
Accepted 9 March 2008
Available online 7 April 2008
Editor: J.-P. Blaizot

ABSTRACT

We explore the formation of diquark bound states and their Bose–Einstein condensation (BEC) in the phase diagram of three-flavor quark matter at nonzero temperature, T, and quark chemical potential, μ. Using a quark model with a four-fermion interaction, we identify diquark excitations as poles of the microscopically computed diquark propagator. The quark masses are obtained by solving a dynamical equation for the chiral condensate and are found to determine the stability of the diquark excitations. The stability of diquark excitations is investigated in the T–μ plane for different values of the diquark coupling strength. We find that diquark bound states appear at small quark chemical potentials and at intermediate coupling strengths. Bose–Einstein condensation of non-strange diquark states occurs when the attractive interaction between quarks is sufficiently strong.

1. Introduction

The one-gluon exchange interaction between quarks is attractive in the color-anti-triplet channel and leads to color superconductivity in cold and dense quark matter [1]. Due to asymptotic freedom of QCD, the strength of the gluon-exchange interaction around the Fermi surface changes with the quark number density. At asymptotically high densities, the interaction is sufficiently weak to apply perturbation theory and the mean-field approximation, and color superconductivity is very similar to standard BCS superconductivity. The gap parameter is $\Delta \sim \mu \exp(-1/g)$, where g is the QCD coupling constant. Quark Cooper pairs are large, with a correlation length $\xi \sim 1/\Delta$ which is parametrically larger than the interparticle distance $d \sim 1/\mu$. On the other hand, at intermediate densities which may be realized in the cores of compact stars and/or in the intermediate stages of heavy-ion collisions, the quark–quark interaction is relatively strong and the properties of the quark Cooper pairs will be modified. In particular, we expect their size to become of the same order as the interparticle distance, $\xi \sim 1/\Delta \sim d$ [2,3]. Moreover, it was argued that, due to the strong coupling, the fluctuations of the diquark-pair field become large around the critical temperature T_c [4] and that they give rise to a pseudogap region in the normal phase above T_c [5,6].

If the quark–quark interaction becomes strong enough before the quarks are confined at lower density, quark Cooper pairs become small enough to be considered as tightly bound diquark states. The color-superconducting ground state of quark matter at low temperature may turn into a Bose–Einstein condensed phase of diquarks [2,3]. Most likely, the transition happens continuously with the change of the density, just like the BCS-BEC crossover in conventional condensed matter and atomic systems [7,8], see also Refs. [9–15]. An interesting property of diquark bound states is that they can exist even above the critical temperature T_c of BEC, up to the dissociation temperature $T_{\rm diss} > T_c$ [8]. If such modes exist in quark matter, they will affect its properties and experimental observables.

In this work, we explore the appearance of bound diquarks and their BEC in the phase diagram of quark matter using a low-energy effective model. This model features an attractive quark–quark interaction with a constant coupling strength G_D that is regarded as a free parameter of the model. We show that diquark bound states appear at low density at intermediate values of G_D. It is also shown that BEC of such diquark states can occur for large values of G_D.

In the normal phase above T_c, the strongest decay mode of diquark bound states is that into a pair of quarks. Since the excitation energy of a quark at rest is $M - \mu$, with M being the mass of the quark, the threshold energy for this decay process is $\omega_{\rm thr} = 2(\bar{M} - \bar{\mu})$, where $\bar{M}$ and $\bar{\mu}$ are the average mass and chemical potential of the quarks in the diquark. Recalling that the energy of the diquark excitations should be positive to ensure the stabil-

* Corresponding author.
E-mail addresses: masky@yukawa.kyoto-u.ac.jp (M. Kitazawa), drischke@th.physik.uni-frankfurt.de (D.H. Rischke), i-shovkovy@wiu.edu (I.A. Shovkovy).

0370-2693/$ – see front matter
doi:10.1016/j.physletb.2008.03.067

ity of the system, one finds that the necessary condition for the existence of stable diquarks is $\omega_{\rm thr} > 0$, or

$$\bar{M} > \bar{\mu}. \tag{1}$$

At $T = T_c$, as we will see later, Eq. (1) is also a sufficient condition [8,9,14]. From Eq. (1), we conclude that the stability of diquark excitations is determined by the quark masses. Quark masses are dynamically generated by chiral symmetry breaking and change as functions of T and μ. In this work, we solve the gap equations for the chiral condensates and incorporate this effect in our calculation. Eq. (1) also indicates that diquarks composed of heavier quarks tend to be more stable than those composed of light quarks, provided they exist at all. One thus expects that diquarks containing a strange quark are more stable than those composed of up and down quarks only.

Usually, BEC is discussed using the canonical ensemble, i.e., the particle number density is fixed as an external parameter. In this work, however, we employ the grand canonical ensemble and draw the phase diagram in the T–μ plane, as is usually done in the literature when exploring the QCD phase diagram [1]. In order to decide whether BEC of diquarks occurs in this ensemble, we regard the region of the superconducting phase satisfying Eq. (1) as Bose–Einstein condensed phase [8,14].

In this exploratory study, we employ a common chemical potential μ for all flavors and colors. For quark matter in compact stars, this is probably not a very good assumption, as the chemical potentials should be determined to satisfy the neutrality and beta-equilibrium conditions. It is known that a rich phase structure can appear under these conditions [16]. However, as we shall see in the following, diquark excitations play an important role even at high temperatures and small chemical potentials in the range relevant for heavy-ion collisions. In this case, our assumption of equal chemical potentials for all quark flavors and colors is applicable to very good approximation.

This statement warrants a few remarks. Thermal model fits of hadron yields at chemical freeze-out show that, because of strangeness and isospin conservation, neither the strangeness chemical potential μ_S nor the isospin chemical potential μ_I are zero. The strangeness chemical potential is nonzero because of associated production channels in hadronic matter at nonzero baryon chemical potential. For quark matter, however, μ_S should be strictly zero if the system has zero strangeness, and we may neglect μ_S. The isospin chemical potential is nonzero because of the initial isospin asymmetry of the colliding nuclei. However, at all collision energies it has been demonstrated [17] that $\mu_B \equiv 3\mu \gg |\mu_I|$. Thus, to leading order we may set $\mu_I = 0$.

We note that parts of the present work have been recently published in Ref. [18]. Here, we go substantially beyond that work by discussing in detail the dependence of the quark masses and the order parameters on the quark chemical potential (Fig. 2), by investigating the dissociation temperatures as function of the diquark coupling strength (Fig. 4), by showing the baryon density as a function of quark chemical potential at zero temperature (Fig. 5), and by computing the equation of state (Fig. 6) which is a necessary input to determine the mass-radius relationship of compact stars via the Tolman–Oppenheimer–Volkov equation. We also note that in Ref. [14] a related study was done, albeit only for two quark flavors and without showing the phase diagram in the T–μ plane (instead, color neutrality, additional vector meson coupling terms, and the chromomagnetic instability were discussed). We agree qualitatively with the conclusions drawn in that work.

The remainder of this work is organized as follows. In Section 2 we present details of our mathematical formalism. In Section 3 we show the numerical results. We conclude this work with a summary in Section 4. Our units are $\hbar = c = k_B = 1$.

2. Formalism

In order to study the phase diagram of quark matter, we employ a three-flavor quark model with four-fermion interactions. The Lagrangian is given by

$$\begin{aligned}\mathcal{L} = {} & \bar{\psi}(i\partial\!\!\!/ - \hat{m})\psi + G_S \sum_{a=0}^{8}\left[(\bar{\psi}\lambda_a\psi)^2 + (\bar{\psi}i\gamma_5\lambda_a\psi)^2\right] \\ & + G_D \sum_{\gamma,c}\left[\bar{\psi}^a_\alpha i\gamma_5\epsilon^{\alpha\beta\gamma}\epsilon_{abc}(\psi_C)^b_\beta\right]\left[(\bar{\psi}_C)^r_\rho i\gamma_5\epsilon^{\rho\sigma\gamma}\epsilon_{rsc}\psi^s_\sigma\right],\end{aligned} \tag{2}$$

where the quark field ψ^a_α has color ($a = r, g, b$) and flavor ($\alpha = u, d, s$) indices. The matrix of current quark masses is given by $\hat{m} = \mathrm{diag}_f(m_u, m_d, m_s)$; $\lambda_0 = \sqrt{2/3}\mathbf{1}$ and λ_a, $a = 1, \ldots, 8$, are the Gell-Mann matrices in flavor space. The charge conjugate spinors are $\psi_C = C\bar{\psi}^T$ and $\bar{\psi}_C = \psi^T C$, where $C = i\gamma^2\gamma^0$ is the charge conjugation matrix. In the following, we only consider diquark condensates and diquark excitations in the color anti-triplet channel. For the numerical calculations, we employ a three-dimensional momentum cutoff Λ. We treat the diquark coupling constant G_D as a free parameter. For the other parameters, we use the values of Ref. [19],[1] $m_u = m_d = 5$ MeV, $m_s = 120$ MeV, $G_S = 6.41$ GeV^{-2} and $\Lambda = 600$ MeV.

We evaluate the thermodynamic potential in the mean-field approximation:

$$\begin{aligned}\Omega = {} & \frac{1}{4G_D}\sum_{c=1}^{3}|\Delta_c|^2 + \frac{1}{8G_S}\sum_{\alpha=1}^{3}(M_\alpha - m_\alpha)^2 \\ & - \frac{T}{2}\sum_n\int\frac{d^3\boldsymbol{p}}{(2\pi)^3}\,\mathrm{Tr}_{\mathrm{D,f,c}}\ln\left[S^{-1}(i\omega_n, \boldsymbol{p})\right],\end{aligned} \tag{3}$$

where the trace is taken over Dirac, flavor, and color indices, $\omega_n = (2n+1)\pi/T$ is the Matsubara frequency for fermions, and

$$M_\alpha = m_\alpha - 4G_S\langle\bar{\psi}_\alpha\psi_\alpha\rangle, \tag{4}$$

$$\Delta_c = 2G_D\langle\bar{\psi}_C P_c\psi\rangle, \tag{5}$$

are the constituent quark masses and the gap parameters for color superconductivity, respectively, with $(P_c)^{\alpha\beta}_{ab} = i\gamma_5\epsilon^{\alpha\beta c}\epsilon_{abc}$. The 72×72 Nambu–Gor'kov propagator is defined by

$$S^{-1}(i\omega_n, p) = \begin{pmatrix} p\!\!\!/ + \mu\gamma_0 - \hat{M} & \sum_\eta P_\eta\Delta_\eta \\ \sum_\eta \gamma^0 P^\dagger_\eta\gamma^0\Delta_\eta & {}^t p\!\!\!/ - \mu\gamma_0 + \hat{M}\end{pmatrix}, \tag{6}$$

with $p\!\!\!/ = i\omega_n\gamma_0 - \boldsymbol{p}\cdot\boldsymbol{\gamma}$ and $\hat{M} = \mathrm{diag}_f(M_u, M_d, M_s)$. The quark chemical potential μ has a common value for all flavors and colors, as mentioned above.

The physical values of the variational parameters Δ_c and M_α satisfy the stationary conditions (the gap equations)

$$\frac{\partial\Omega}{\partial\Delta_c} = 0 \quad \text{and} \quad \frac{\partial\Omega}{\partial M_\alpha} = 0. \tag{7}$$

As we shall see later, the color-superconducting phase transitions at nonzero temperature are of second order. Thus, the critical temperatures are determined by solving the following equation:

$$\frac{1}{\Delta_c}\frac{\partial\Omega}{\partial\Delta_c}\bigg|_{\Delta_c=0} = 0. \tag{8}$$

We shall see later that this equation determines the poles of the diquark propagator at vanishing energy and momentum.

[1] In this reference, since the same parameters are employed, the phase structure is completely the same as in Fig. 1, except for the lines for $T^c_{\rm diss}$, which were not shown in that reference.

Since up and down flavors are degenerate in our model, we always have $M_u = M_d$ and $\Delta_1 = \Delta_2$. In the following, we refer to the phase with $\Delta_3 \neq 0$ and $\Delta_{1,2} = 0$ as the 2SC phase; the phase with $\Delta_3 \neq 0$ and $\Delta_{1,2} \neq 0$ is the CFL phase [1]. Unpaired quark matter has $\Delta_1 = \Delta_2 = \Delta_3 = 0$. Because of the explicit chiral symmetry breaking by the nonzero current quark masses, the chiral condensates $\langle\bar{\psi}_i\psi_i\rangle$ never vanish.

At nonzero temperature, the order-parameter fields, $\Delta_c(\boldsymbol{x},t)$ and $M_\alpha(\boldsymbol{x},t)$ have fluctuations around the values determined by the mean-field approximation. In the following, we consider the amplitude fluctuations of $\Delta_c(\boldsymbol{x},t)$ in unpaired quark matter. The propagation of the fluctuations is characterized by the retarded propagator

$$\begin{aligned} &D_c^R(\boldsymbol{x},t;\boldsymbol{x}',t') \\ &\quad = -i\theta(t-t')\left\langle\left[\bar{\psi}(\boldsymbol{x},t)P_c\psi_C(\boldsymbol{x},t),\bar{\psi}_C(\boldsymbol{x}',t')P_c\psi(\boldsymbol{x}',t')\right]\right\rangle \\ &\quad = \int\frac{d^3\boldsymbol{p}\,d\omega}{(2\pi)^4}D_c^R(\boldsymbol{p},\omega)\mathrm{e}^{-i\omega(t-t')}\mathrm{e}^{i\boldsymbol{p}\cdot(\boldsymbol{x}-\boldsymbol{x}')}, \end{aligned} \tag{9}$$

where $c = 1, 2$, and 3 correspond to the down-strange, up-strange, and up–down diquark fields, respectively. In the random-phase approximation, the diquark propagator is given by

$$D_c^R(\boldsymbol{p},\omega) = \frac{1}{2}\frac{Q_c^R(\boldsymbol{p},\omega)}{1+G_D\,Q_c^R(\boldsymbol{p},\omega)}, \tag{10}$$

where $Q_c^R(\boldsymbol{p},\omega)$ is the one-loop quark–quark polarization function. In the imaginary-time formalism, it is given by

$$\begin{aligned} &\mathcal{Q}_c(\boldsymbol{p},i\nu_n) \\ &\quad = -2T\sum_m\int\frac{d^3\boldsymbol{q}}{(2\pi)^3} \\ &\qquad\times\mathrm{Tr}_{\mathrm{D,f,c}}\left[P_cS_0(\boldsymbol{p}-\boldsymbol{q},i\nu_n-i\omega_m)P_cCS_0^T(\boldsymbol{q},i\omega_m)C\right], \end{aligned} \tag{11}$$

where $\nu_n = 2\pi n/T$ denotes the Matsubara frequency for bosons, and $S_0(\boldsymbol{p},i\omega_n) = [\not{p}+\mu\gamma_0-\hat{M}]^{-1}$. Taking the analytic continuation, $Q_c^R(\boldsymbol{p},\omega) = \mathcal{Q}_c(\boldsymbol{p},i\nu_n)|_{i\nu_n\to\omega+i\eta}$, we obtain

$$\begin{aligned} Q_c^R(\boldsymbol{p},\omega) = -2\sum_{\beta,\gamma=1}^{3}\left|\epsilon^{c\beta\gamma}\right|\int\frac{d^3\boldsymbol{q}}{(2\pi)^3} &\times\sum_{s,t=\pm}\frac{(sE_\beta+tE_\gamma)^2-|\boldsymbol{p}|^2-(\delta M_c)^2}{stE_\beta E_\gamma} \\ &\times\frac{f(tE_\gamma-\mu)-f(-sE_\beta+\mu)}{\omega+2\mu-sE_\beta-tE_\gamma+i\eta}, \end{aligned} \tag{12}$$

where $E_\beta = \sqrt{|\boldsymbol{q}-\boldsymbol{p}|^2+M_\beta^2}$, $E_\gamma = \sqrt{|\boldsymbol{q}|^2+M_\gamma^2}$, $\delta M_c = |M_\beta - M_\gamma|$, and $f(E) = [\exp(E/T)+1]^{-1}$ is the Fermi distribution function. The imaginary part of $Q_c^R(\boldsymbol{p},\omega)$ denotes the difference of decay and production rates of the diquark field. At $\boldsymbol{p} = 0$, it is given by

$$\begin{aligned} &\mathrm{Im}\,Q_c^R(\boldsymbol{0},\omega) \\ &\quad = 2\pi\sum_{\beta,\gamma=1}^{3}\left|\epsilon^{c\beta\gamma}\right|\int\frac{d^3\boldsymbol{q}}{(2\pi)^3}\frac{(\omega+2\mu)^2-(\delta M_c)^2}{E_\beta E_\gamma} \\ &\qquad\times\left\{-\left[(1-f_\beta^+)(1-f_\gamma^+)-f_\beta^+f_\gamma^+\right]\delta(\omega+2\mu-E_\beta-E_\gamma)\right. \\ &\qquad+\left[(1-f_\beta^-)(1-f_\gamma^-)-f_\beta^-f_\gamma^-\right]\delta(\omega+2\mu+E_\beta+E_\gamma) \\ &\qquad-\left[f_\beta^-(1-f_\gamma^+)-(1-f_\beta^-)f_\gamma^+\right]\delta(\omega+2\mu+E_\beta-E_\gamma) \\ &\qquad\left.-\left[f_\beta^+(1-f_\gamma^-)-(1-f_\beta^+)f_\gamma^-\right]\delta(\omega+2\mu-E_\beta+E_\gamma)\right\}, \end{aligned} \tag{13}$$

where $f_\alpha^\pm = \{\exp[(E_\alpha\mp\mu)/T]+1\}^{-1}$. The first (second) term in the bracket in Eq. (13) includes the decay processes of the diquark into two quarks (anti-quarks) and takes nonzero values at $\omega > 2\bar{M}_c - 2\mu$ ($\omega < -2\bar{M}_c - 2\mu$), with $\bar{M}_c = (M_\beta + M_\gamma)/2$. The third and fourth terms represent Landau damping of the diquark. These terms become nonzero at $-\delta M_c - 2\mu < \omega < \delta M_c - 2\mu$.

The poles of the diquark propagator D_c^R are determined by solving $D_c^R(\boldsymbol{p},\omega)^{-1} = 0$, or equivalently

$$1 + G_D\,Q_c^R(\boldsymbol{p},\omega) = 0, \tag{14}$$

in the complex-energy plane. Applying $\omega = |\boldsymbol{p}| = 0$ to this equation, one can easily show that Eq. (14) is equivalent to the critical condition Eq. (8). Therefore, $D_c^R(\boldsymbol{p},\omega)$ has a pole at the origin at $T = T_c$ of the second-order transition. This property is known as the Thouless criterion in condensed matter physics [20]. Above T_c, the pole moves continuously from the origin to the fourth quadrant. This mode is called the soft mode. If $\bar{M}_c < \mu$ at $T = T_c$, $\omega = 0$ is in the continuum of the decay process into two quarks and the imaginary part at the pole starts growing just above T_c [4]. When $\bar{M}_c > \mu$, on the other hand, the soft mode is stable against spontaneous breaking into a pair of quarks and the pole moves on the real axis in the vicinity of T_c. This mode is nothing but a bound state of two quarks [8]. As T increases, the pole eventually arrives at the threshold of the decay process into two quarks $\omega_{\mathrm{thr}} = 2(\bar{M}_c - \mu)$ at the dissociation temperature T_{diss}, and the soft mode is no longer a bound state at $T > T_{\mathrm{diss}}^c$. Since the pole is at ω_{thr} at T_{diss}^c, the dissociation temperature is determined by solving

$$1 + G_D\,Q_c(\boldsymbol{p}=0,\omega_{\mathrm{thr}})|_{T=T_{\mathrm{diss}}^c} = 0. \tag{15}$$

Although the diquark modes can acquire decay rates due to Landau damping, i.e., the third and fourth term in Eq. (13), our numerical results show that the soft modes never appear in the range of energies where Landau damping is nonzero. Therefore, these processes do not contribute to the decay rate of the soft modes in the parameter range employed in the present study. There can appear another pole of $D_c^R(\boldsymbol{p},\omega)$ instead of the soft mode at the energy $-2\bar{M}_c - 2\mu < \omega < -\delta M_c - 2\mu$. This mode does not have a decay rate and should be identified as a bound anti-diquark [9]. For lower μ, thermal excitations of bound anti-diquarks play an important role.

If bound diquarks are formed at $T = T_c$, it is natural to identify the color-superconducting phase below T_c as a Bose–Einstein condensed phase of diquark bound states [8]. In the following, therefore, we regard the color-superconducting phase satisfying $\bar{M}_c < \mu$ as a Bose–Einstein condensate. Notice, however, that this is just a rough guide to separate the BEC and BCS regions; these two limits are connected continuously and there is no sharp phase boundary between them [8].

3. Numerical results

In this section, we show the phase diagram in the T–μ plane for several values of the diquark coupling G_D. In Fig. 1, we first discuss the case $G_D/G_S = 0.75$, which is a value commonly used in the literature [1,19]. The bold and thin solid lines represent first- and second-order phase transitions, respectively. One sees that there appear two types of color-superconducting phases, the 2SC and CFL phase, at high μ and low T. At $T = 0$, these phases are separated by a first-order phase transition. The first-order transition terminates at a critical point for some nonzero value of temperature. The dissociation temperatures of diquark bound states T_{diss}^c are shown by the dashed lines. We see that there exists a region at small chemical potential where bound diquarks are formed.

In order to see whether diquark states undergo BEC, we plot the conditions $\mu = \bar{M}_c$ by the dash-dotted lines in Fig. 1; the regions to the left of these lines satisfy $\mu < \bar{M}_c$. We see that these

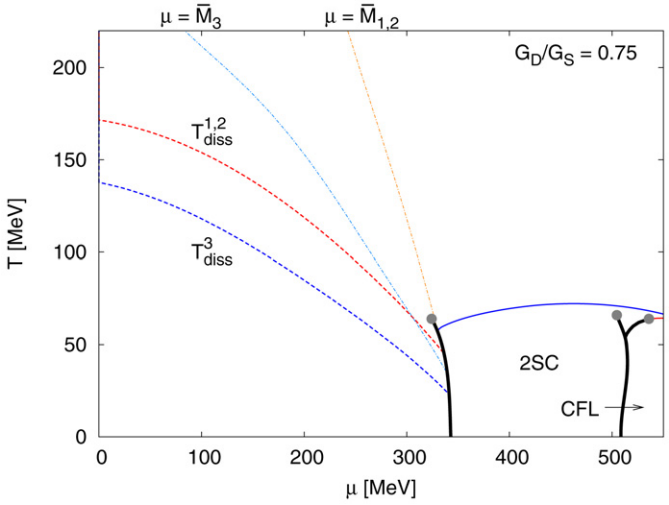

Fig. 1. The phase diagram in the T–μ plane for $G_D/G_S = 0.75$. The bold and thin solid lines represent first- and second-order phase transitions. The dashed lines denote the dissociation temperature of up–down diquark states, $T^3_{\rm diss}$, and up-strange and down-strange diquark states, $T^{1,2}_{\rm diss}$. The conditions $\mu = \bar{M}_c$ are satisfied along the dash-dotted lines.

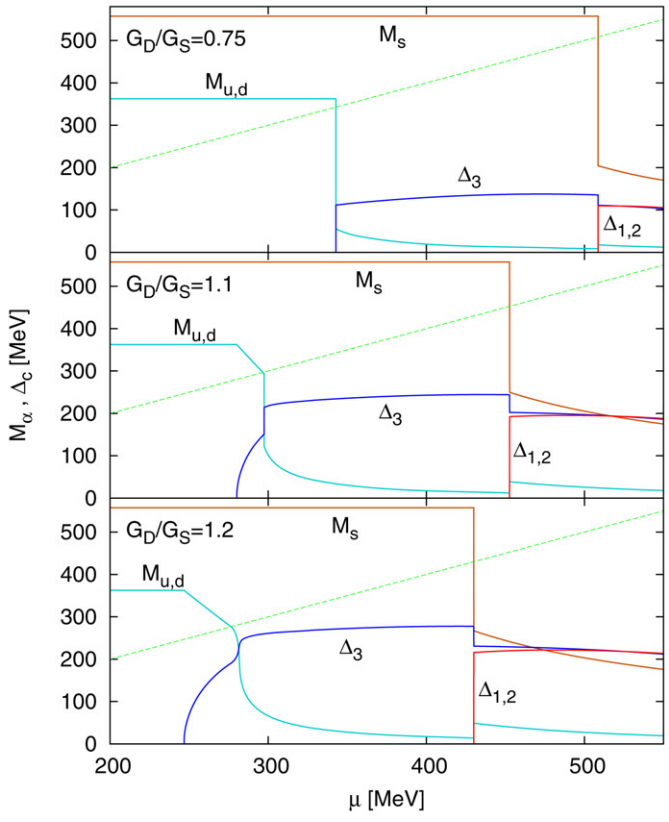

Fig. 2. Order parameters M_α and Δ_c at $T = 0$ as functions of μ for various values of the diquark coupling $G_D/G_S = 0.75$, 1.1 and 1.2. The chemical potential is shown by the dashed line.

lines terminate at the first-order transition and we do not have a color-superconducting phase satisfying $\mu < \bar{M}_c$. In other words, BEC does not appear for this value of G_D/G_S. The behavior of $\bar{M}_c$ and Δ_c as functions of μ at $T = 0$ are shown in the upper panel of Fig. 2. One observes that $\bar{M}_3 = M_{u,d}$ has a discontinuity at $\mu \simeq 343$ MeV corresponding to a first-order transition, and $\bar{M}_3$ is larger than μ to the left of the discontinuity. The diquark

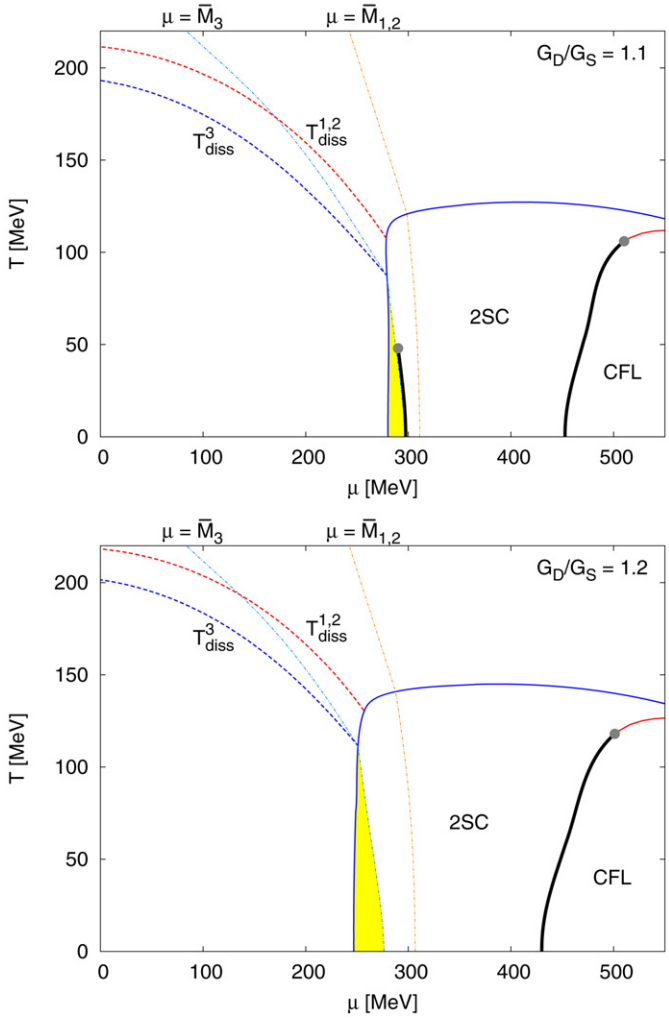

Fig. 3. The phase diagram in the T–μ plane for relatively strong diquark couplings $G_D/G_S = 1.1$ and 1.2. BEC of up–down diquarks occurs in the shaded area.

condensate Δ_3 assumes nonzero values only for $\mu > \bar{M}_3$. This is a typical property at weak coupling; when $\mu > \bar{M}_3$, the Fermi surfaces of up and down quarks exist and the Cooper instability leads to a diquark condensate, while if not, the ground state is nothing other than the vacuum.

It is worth mentioning that bound diquarks appear in the phase diagram even though BEC does not exist in the phase diagram. The diquark coupling used in Fig. 1 is strong enough to form bound diquarks, but it is still too weak to lead to their BEC.

Next, we show the phase diagrams with much stronger diquark couplings. In Fig. 3, the phase diagrams with $G_D/G_S = 1.1$ and 1.2 are shown. We see that, as G_D becomes larger, the regions of the 2SC and CFL phases expand toward lower μ and higher T. For $G_D/G_S = 1.1$, there appears BEC of up–down diquarks in the region of the 2SC phase satisfying $\mu < \bar{M}_3$, shown by the shaded area in Fig. 3. The BEC region becomes wider for $G_D/G_S = 1.2$. One also observes that the dissociation temperatures $T^c_{\rm diss}$ become higher as G_D increases. In the phase diagrams in Fig. 3, $T^c_{\rm diss}$ at $\mu = 0$ are comparable or much higher than the critical temperature of the QCD phase transition, which is predicted to be in the range $T_c \sim 150$–190 MeV in lattice QCD simulations [21]. This result shows that diquark bound states can exist even in the quark–gluon plasma phase provided the diquark coupling is sufficiently strong.

In order to see the diquark coupling dependence of the dissociation temperatures, we show $T^c_{\rm diss}$ at $\mu = 0$ as functions of G_D/G_S

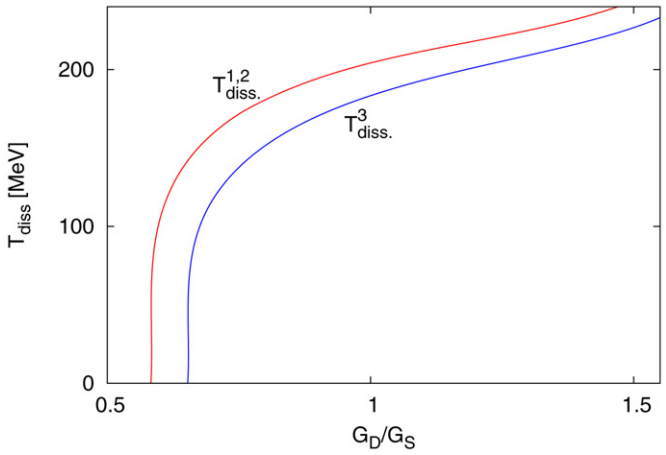

Fig. 4. Dissociation temperatures of up–down diquarks $T^3_{\rm diss}$, and up-strange and down-strange diquarks $T^{1,2}_{\rm diss}$.

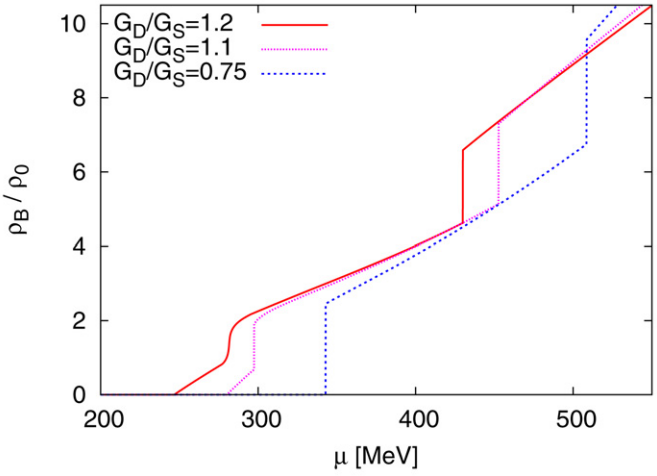

Fig. 5. The baryon number density ρ_B for $T = 0$ and $G_D/G_S = 0.75$, 1.1 and 1.2.

in Fig. 4. At weak coupling, $T^c_{\rm diss} = 0$ and bound diquarks do not exist. As G_D/G_S becomes larger, $T^c_{\rm diss}$ eventually become nonzero and increase rapidly. The dissociation temperatures for diquarks including the strange quark, $T^{1,2}_{\rm diss}$, are always higher than that for the up–down diquark. This feature comes from the difference of the threshold energy $2(\bar{M}_c - \mu)$.

The other interesting feature shown in Figs. 1 and 3 is the behavior of the line of first-order phase transitions. The first-order phase transition at lower density is shorter for $G_D/G_S = 1.1$ than that for $G_D/G_S = 0.75$, and disappears at $G_D/G_S = 1.2$. To understand this behavior, we display the order parameters for $G_D/G_S = 1.1$ and 1.2 in the middle and lower panels of Fig. 2, respectively. The figure shows that, as G_D becomes larger, Δ_c increase while the quark masses $\bar{M}_c$ become smaller, and the discontinuity of $\bar{M}_3$ disappears at $G_D/G_S = 1.2$. The decrease of $\bar{M}_c$ can be understood as the interplay between the chiral and diquark condensates [22]: the energy gain due to diquark condensation is proportional to the surface area of the Fermi sphere. Since the radius of the Fermi sphere is $p_F = \sqrt{\mu^2 - M^2}$, the condensation energy increases when M decreases. Since the masses of quarks are suppressed as G_D becomes larger, the lines for $\mu = \bar{M}_c$ and the region of BEC move toward lower μ.

It is of interest to consider the effects of BEC on thermodynamic quantities. In Fig. 5, we show the baryon number density $\rho_B = -(\partial\Omega/\partial\mu)/3$ at $T = 0$ as a function of μ for $G_D/G_S = 0.75$, 1.1 and 1.2. For $G_D/G_S = 0.75$ and 1.1, there exist two discontinuities of ρ_B corresponding to first-order transitions. While ρ_B vanishes below the first first-order transition for $G_D/G_S = 0.75$, ρ_B takes nonzero values even in this region for $G_D/G_S = 1.1$. This region corresponds to BEC, and the density there is dominated by diquarks. For $G_D/G_S = 1.2$, the first-order transition at lower μ disappears and ρ_B varies continuously. The density ρ_B in the 2SC phase is higher for larger G_D/G_S. The larger diquark gap Δ_3 induced by strong coupling as well as smaller quark masses $M_{u,d}$ contribute to this behavior.

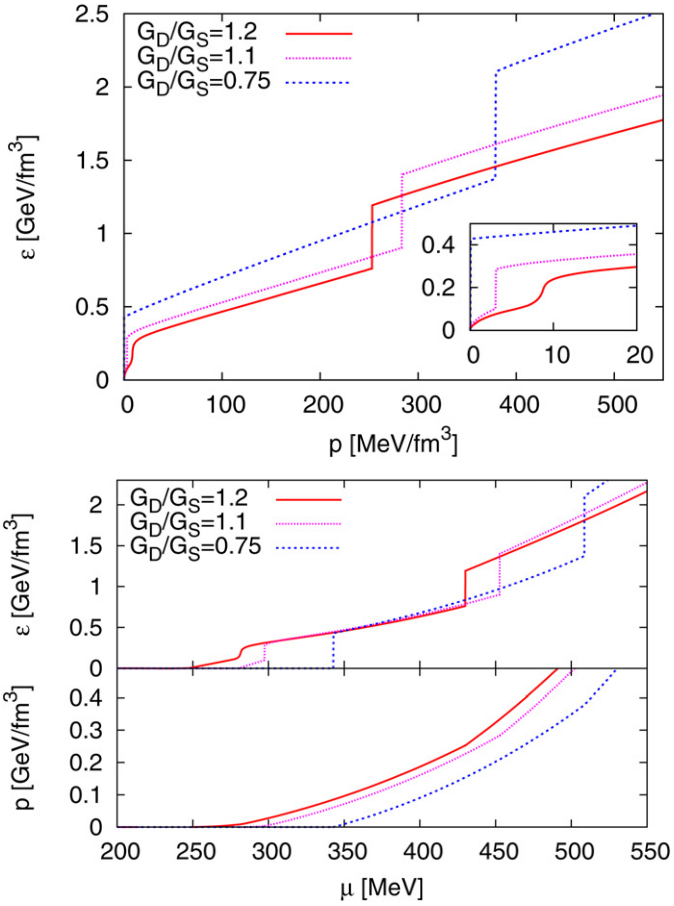

Fig. 6. The equation of states for $T = 0$ and $G_D/G_S = 0.75$, 1.1 and 1.2 (upper panel), and the energy density ϵ and pressure p as functions of μ for $T = 0$ (lower panel).

The upper panel of Fig. 6 shows the equation of state (EoS) at $T = 0$, i.e., energy density $\epsilon = \Omega + \mu\rho$ as a function of pressure $p = -\Omega$, for the three values of diquark coupling strength: $G_D/G_S = 0.75$, 1.1 and 1.2. (The region of small pressure is depicted in the small insert in the figure.) Both ϵ and p as functions of μ are shown in the lower panel of Fig. 6. The key feature to be noted from the dependence of the EoS on G_D/G_S is that it becomes harder with increasing coupling. This is violated only in an intermediate range where the 2SC-CFL phase transition occurs. (Note that the density of the 2SC-CFL transition decreases with increasing coupling, as expected.)

Finally, let us consider the phase diagram for extremely large diquark coupling. In Fig. 7, we show the phase diagram for $G_D/G_S = 1.5$. The 2SC and CFL phases become much wider toward lower μ and higher T, and $T^c_{\rm diss}$ increases further. The region of BEC of up–down diquarks also becomes wide. We do not obtain a region in the CFL phase satisfying $\mu > \bar{M}_{1,2}$, i.e., BEC of up-strange and down-strange diquarks does not occur for $G_D/G_S \leqslant 1.5$. If the diquark coupling is further increased, the vacuum, i.e., $T = \mu = 0$,

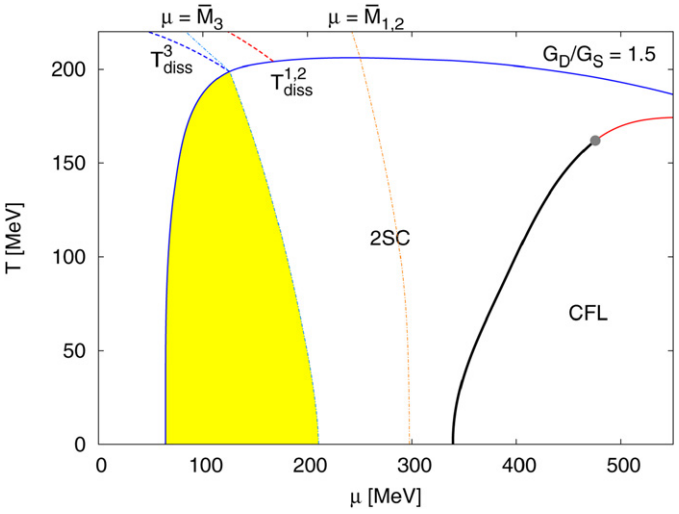

Fig. 7. The phase diagram in the T–μ plane for extremely strong diquark coupling $G_D/G_S = 1.5$.

eventually becomes a Bose–Einstein condensate of diquark states, which is clearly unphysical.

4. Summary and discussions

In this Letter, we explored the phase diagram of three-flavor quark matter focusing on the appearance of diquark bound states and their Bose–Einstein condensation under variation of the diquark coupling constant G_D. We found that diquark states can appear at small μ and (probably realistically large) intermediate values of the diquark coupling, while BEC of up–down diquarks is realized for (probably unphysically) large values of the diquark coupling. The dissociation temperatures of diquarks become higher as G_D increases. The model employed in the present study does not include the effect of confinement. In QCD, however, colored objects are confined at lower T and μ. Therefore, it is not clear that the bound diquarks and their BEC, which manifest itself at lower T and μ in our model, appear in the QCD phase diagram. It is, however, worth mentioning that at strong coupling the dissociation temperatures could be higher than the critical temperature of the deconfinement transition determined by lattice QCD [21]. This result implies that diquark bound states can exist in the quark–gluon plasma phase.

In this work, we employed the random-phase approximation for the calculation of the diquark propagator. In this approximation, the propagators in the polarization function Eq. (11) are those for non-interacting quarks, i.e., the effect of diquark excitations is not self-consistently incorporated. An extension of the present work to include this effect is an interesting subject for further study, because we expect that the formation of diquark bound states would modify the result especially at high temperatures. Similarly, the mean-field approximation used to draw the phase diagram is no longer applicable due to the existence of well-developed soft modes in a strongly coupled system. The incorporation of these effects has already been partially made in Ref. [15].

Acknowledgements

M.K. thanks H. Abuki and T. Kunihiro for discussions.

References

[1] K. Rajagopal, F. Wilczek, hep-ph/0011333;
M. Alford, Annu. Rev. Nucl. Part. Sci. 51 (2001) 131;
T. Schäfer, hep-ph/0304281;
D.H. Rischke, Prog. Part. Nucl. Phys. 52 (2004) 197, nucl-th/0305030;
H.-C. Ren, hep-ph/0404074;
M. Huang, hep-ph/0409167;
I.A. Shovkovy, Found. Phys. 35 (2005) 1309, nucl-th/0410091.
[2] M. Matsuzaki, Phys. Rev. D 62 (2000) 017501, hep-ph/9910541.
[3] H. Abuki, T. Hatsuda, K. Itakura, Phys. Rev. D 65 (2002) 074014, hep-ph/0109013.
[4] M. Kitazawa, T. Koide, T. Kunihiro, Y. Nemoto, Phys. Rev. D 65 (2002) 091504, nucl-th/0111022.
[5] E. Babaev, Int. J. Mod. Phys. A 16 (2001) 1175, hep-th/9909052.
[6] M. Kitazawa, T. Koide, T. Kunihiro, Y. Nemoto, Phys. Rev. D 70 (2004) 056003, hep-ph/0309026;
M. Kitazawa, T. Koide, T. Kunihiro, Y. Nemoto, Prog. Theor. Phys. 114 (2005) 205, hep-ph/0502035.
[7] A.J. Leggett, J. Phys. 41 (1980) C7.
[8] P. Nozières, S. Schmitt-Rink, J. Low Temp. Phys. 59 (1985) 195.
[9] Y. Nishida, H. Abuki, Phys. Rev. D 72 (2005) 096004, hep-ph/0504083.
[10] K. Nawa, E. Nakano, H. Yabu, Phys. Rev. D 74 (2006) 034017, hep-ph/0509029.
[11] H. Abuki, Nucl. Phys. A 791 (2007) 117, hep-ph/0605081.
[12] J. Deng, A. Schmitt, Q. Wang, Phys. Rev. D 76 (2007) 034013, nucl-th/0611097.
[13] D. Ebert, K.G. Klimenko, Phys. Rev. D 75 (2007) 045005, hep-ph/0611385.
[14] G.F. Sun, L. He, P. Zhuang, Phys. Rev. D 75 (2007) 096004, hep-ph/0703159.
[15] L. He, P. Zhuang, Phys. Rev. D 76 (2007) 056003, arXiv: 0705.1634 [hep-ph].
[16] I. Shovkovy, M. Huang, Phys. Lett. B 564 (2003) 205, hep-ph/0302142;
M. Alford, C. Kouvaris, K. Rajagopal, Phys. Rev. Lett. 92 (2004) 222001, hep-ph/0311286;
S.B. Rüster, I.A. Shovkovy, D.H. Rischke, Nucl. Phys. A 743 (2004) 127, hep-ph/0405170;
K. Iida, T. Matsuura, M. Tachibana, T. Hatsuda, Phys. Rev. D 71 (2005) 054003, hep-ph/0411356;
S.B. Rüster, V. Werth, M. Buballa, I.A. Shovkovy, D.H. Rischke, Phys. Rev. D 72 (2005) 034004, hep-ph/0503184;
D. Blaschke, S. Fredriksson, H. Grigorian, A.M. Öztaş, F. Sandin, Phys. Rev. D 72 (2005) 065020, hep-ph/0503194.
[17] P. Braun-Munzinger, I. Heppe, J. Stachel, Phys. Lett. B 465 (1999) 15, nucl-th/9903010.
[18] M. Kitazawa, D.H. Rischke, I.A. Shovkovy, Prog. Theor. Phys. Suppl. 168 (2007) 389, arXiv: 0707.3966 [nucl-th].
[19] M. Buballa, M. Oertel, Nucl. Phys. A 703 (2002) 770, hep-ph/0109095.
[20] D.J. Thouless, Ann. Phys. 10 (1960) 553.
[21] M. Cheng, et al., Phys. Rev. D 74 (2006) 054507, hep-lat/0608013;
Y. Aoki, et al., Phys. Lett. B 643 (2006) 46, hep-lat/0609068.
[22] M. Kitazawa, T. Koide, T. Kunihiro, Y. Nemoto, Prog. Theor. Phys. 108 (2002) 929, hep-ph/0207255, and references therein.